Adaptive Fractal Quadtree Approach for Efficient Drone-Based Construction Site Safety Inspection

Marvin Cheng[1], Ci-Jyun Liang[2], and Hugo Camargo[1]

[1]Division of Safety Research, National Institute for Occupational Safety and Health, USA
[2]Department of Civil Engineering, Stony Brook University, USA
MCheng@cdc.gov, Ci-Jyun.Liang@stonybrook.edu, HCamargo@cdc.gov

Abstract –

This study presents a novel approach for optimizing the flight paths of multiple drones during construction site inspection and monitoring by leveraging image compression techniques, specifically the fractal quadtree method. Traditional path planning methods often fail to account for varying levels of complexity across the construction site, leading to inefficiencies in energy consumption and scanning time. By applying the fractal quadtree approach, we dynamically adapt grid sizes based on the complexity of the initial captured site images, allowing drones to prioritize more intricate areas while minimizing focus on simpler regions. Simulation results demonstrate that this method efficiently reduces the number of required scans compared to conventional approaches, significantly improving the overall efficiency of construction site inspections. The integration of this adaptive path planning strategy provides a scalable and time-saving solution for hazard identification and site monitoring, ensuring more efficient use of drone resources.

Keywords –

Path planning; Safety; Drones; Fractal Algorithm

1 Introduction

Many construction companies are increasingly recognizing the benefits of incorporating drones and unmanned aerial vehicles (UAVs) into their operations [1, 2]. These devices are used to monitor construction progress [3] and inspect structural conditions of civil infrastructures [4] based on 3D reconstruction models. They can also be used to identify hazardous conditions on-site, such as missing personal protective equipment for work at height, and to generate safety warnings for workers [5]. Timely information about nearby hazards is essential for construction workers to ensure their safety. Therefore, drones and UAVs that can quickly and thoroughly scan the entire construction site are crucial [6]. However, deploying a fleet of drones and designing efficient flight paths across construction sites has posed challenges. Existing drone monitor and inspection methods are focused on how to identify the best flight path based on user's experience and 3D reconstruction model quality [3], [4]. Optimizing flight paths is crucial to saving time and energy; for example, Yang et al. [7] proposed an ant colony optimization approach to determine the flight path for digital terrain model reconstruction based on user-defined area, image overlap, and battery limit. In addition, existing methods usually do not consider multiple-drone scenarios in optimization process and assume using a single drone. Traditional flight pattern design methods, such as zigzag or grid-based approaches [8], apply uniform scanning across the entire site and do not account for the varying complexity of different areas. As a result, they can lead to inefficient resource utilization, redundant scans, and even missed critical safety hazards in more complex regions.

In contrast, applying image compression techniques, such as the fractal quadtree method [9], provides a more efficient solution for drone path planning during surface monitoring of construction sites. This approach has been successfully used in adaptive path planning for scanning microscopes [10], [11] robot path planning [12], and trajectories for aerial coverage [13], enabling effective scanning of both complex and simple geometric shapes with different resolutions. By dynamically adjusting the grid sizes based on the visual complexity of different regions, this approach focuses the drones' efforts on areas that require more detailed scanning. Consequently, by dynamically adjusting grid sizes based on the complexity of surface conditions, the proposed fractal quadtree approach (FQA) may allow for better resource allocation, faster coverage, and improved accuracy, as the drones can spend more time in high-risk or complex areas while minimizing redundant scans in simpler zones.

2 Safety Inspection with Drones

To effectively utilize drones to assess safety risks in construction, they must be equipped with high-resolution cameras, GPS for precise localization, and an optimized angle of view to capture fine details across varying site conditions. The clarity of these images primarily depends on two factors: the resolution of the camera and the drone's Ground Sampling Distance (GSD) above the target area. These variables determine the number of pixels captured per unit length in site imagery, which may vary across different areas of interest. However, high-resolution footage is not always required uniformly across all zones; in areas with minimal construction activity, less detailed scrutiny is sufficient compared to zones with intense building operations.

2.1 Flight Altitude and Resolution of Camera

Drones used for hazard inspection on construction sites should be equipped with two cameras: a forward-facing camera for navigation and a downward-facing camera for capturing site images (Figure 1). These cameras can be combined using a gimbal mechanism to reduce the number of sensors the drone needs to carry.

To examine the relationship among the map resolution of the acquired images, the drone's altitude, or ground sampling distance (GSD), and the resolution of the camera used, a geometric relationship can be applied. As illustrated in Figure 1, the visible range of the camera can be easily derived from this geometric configuration. In this setup, the downward-facing camera's field of view (FOV) angle determines the number of pixels per unit length and area based on its resolution at various GSDs. The drone's visible range at a given GSD is determined by the camera's FOV angle, while the pixel density per unit length is governed by the camera's physical resolution as well as GSD. Given the camera resolution and flying altitude, the visible range of each image can be calculated, allowing the total coverage of the construction site to be determined and divided into a grid. Table 1 provides the visible ranges and image resolutions at specified GSDs.

Table 1 Covered visible ranges and image resolutions on the targeted area at specified GSDs.

Camera resolution			720p	1080p
FOV	GSD (m)	Visible range (m)	Pixels / meter	Pixels / meter
90°	10	20 m	36	54
	20	40 m	18	27
	30	60 m	12	18
	40	80 m	9	13.50
120°	10	34.64 m	20.78	31.18
	20	69.28 m	10.39	15.59
	30	103.92 m	6.93	10.39
	40	138.56 m	5.20	7.79

3 Resolution Adjustment and Flight Path Planning of Swarming Drones

Swarming drones involve multiple drones working collaboratively and autonomously in a coordinated manner to perform tasks. To ensure that drones gather useful information across an entire construction site, their visible range and flight pattern had to be defined. In this study, three approaches were examined. Two of the approaches required the drones to maintain a fixed resolution for the captured images, including: 1) random walk approach [14], and 2) zigzag flight path planning. The third approach used an adjustable resolution based on a fractal quadtree approach (FQA). This section explores each approach and outlines the corresponding flight paths.

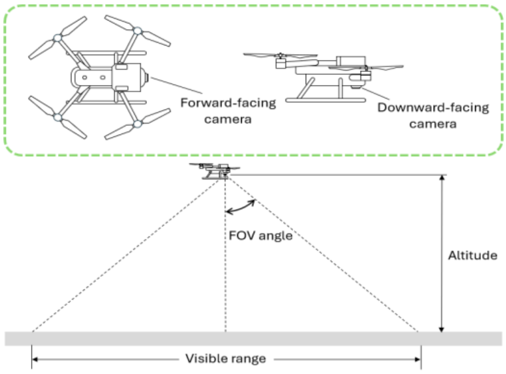

Figure 1. Geometric relationship between FOV angle, altitude, and visible range of the downward-facing camera used by a drone.

3.1 Random Walk Approach

One of the simplest methods for controlling drone behavior is to allow the drones to swarm randomly within a designated map, navigating in various directions across the targeted construction site. The primary advantage of the random walk approach is that the drones only need to communicate for collision avoidance, eliminating the need for coordinated communication or pre-programmed flight paths, which simplifies the overall operation. The images captured by the drones can be stitched together to identify potential hazards. However, this approach can be time-consuming for the drones to cover the entire area, as random flight patterns may result in insufficient coverage and overlap, leading to delays before the full site is scanned. Additionally, since the drones are not coordinated, some areas may receive more attention than necessary, while others might be underexplored. The starting location of the drones, whether random or fixed, does not significantly affect the total time required to complete the scan, but the overall efficiency remains lower compared to more structured flight patterns.

With the random walk theory, the flight pattern can be modeled as a two-dimensional random walk on a grid or a continuous space. Figure 2 demonstrates the possible movements using the random walk method. Each drone makes a series of steps, where each step is determined by a random direction. We assume that the drone's movement direction follows a uniform distribution in the random walk approach, with random starting positions. Figure 3 illustrates the flight paths of two selected drones (out of a total of 50 drones in the simulation) navigating a 100 × 100 grid area during the process of a full scan.

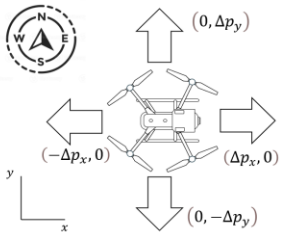

Figure 2. Flight pattern of random walk approach.

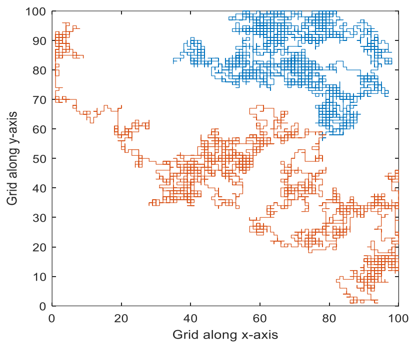

Figure 3. Flight trajectories of two selected drones using random walk approach (50 drones deployed in an area with 100 × 100 cells).

3.2 Zigzag Flight Path Planning

To ensure the image of the targeted construction site can be captured within a predictable timeframe, the zigzag approach can be a versatile option. In this approach, the area is divided proportionally among the total number of drones, allowing the time required to cover the entire site to be easily estimated. By following predefined zigzag paths, the drones systematically sweep through their assigned zones, ensuring full coverage.

In the zigzag approach, the construction site is divided into equal sections for each of the N_D drones, with each drone responsible for scanning a designated portion of the total area, A_S. The total area can be represented as a rectangle or grid of dimensions $L \times W$, where L is the length and W is the width of the site. Thus, the area each drone must cover can be calculated as

$$A_{drone} = \frac{A_S}{N_D} = \frac{L \times W}{N_D}. \quad (1)$$

In this case, the path for each drone is defined by a series of horizontal or vertical zigzag motions across their respective areas.

The path length for each drone depends on the shape of its assigned area. Assuming that the drone moves in a horizontal zigzag pattern, the path length per section for a drone covering an area of $L_{region} \times W_{region}$ is determined by the number of back-and-forth passes required to cover the width of the area. The total length of the path l_{drone} for each drone can be approximated as

$$l_{drone} = \left(L_{region} + 1\right) \cdot \frac{W_{region}}{\Delta p}. \quad (2)$$

where L_{region} is the length of the area each drone covers, W_{region} is the width of the area each drone covers, Δp (Δp_x or Δp_y) is the distance between consecutive passes in the zigzag path. One advantage of the zigzag method is its efficiency. With clearly defined paths, drones can avoid redundant overlap, minimizing wasted time and ensuring that each section of the site is inspected. This structured approach also allows for better time management and straightforward coordination between drones. Moreover, the predictable nature of this method simplifies post-processing, as the images can be stitched together more seamlessly. However, the effectiveness of the zigzag pattern is influenced by the starting positions of the drones. If the drones are not deployed from optimal locations, some may need more time to reach their designated zones, leading to uneven coverage and potential delays. Additionally, the rigid path planning might be less adaptable to irregularly shaped construction sites or areas with obstacles, reducing flexibility compared to more dynamic flight patterns. Overall, the zigzag approach offers a reliable and efficient solution for structured environments, making it a preferred choice when speed and predictability are critical.

3.3 Fractal Quadtree Approach

As noted in the previous section, the visible range of a drone changes with its altitude, affecting the grid sizes used for mapping the targeted area. Image processing techniques using FQA offer a way to dynamically adjust these grid sizes based on the complexity of the construction site surface. Instead of applying a uniform grid across the entire site, this technique adapts the grid resolution according to the visual details captured in lower-resolution images. In areas with lower complexity, such as inactive or open zones, larger grid sizes are used for faster scanning. In contrast, regions with higher complexity, such as those with active construction, are subdivided into smaller grids to capture finer details.

3.3.1 Iterated Function System

In a fractal process, the theory of iterated function systems (IFS) is applied, serving as the foundation for fractal processing techniques [9]. In the application for a construction site, IFS employs affine transformations to capture the relationships between different sections of the image S of the target construction site captured by the downward-facing camera. By using the transformations, it can define and represent areas with complex structures efficiently. Affine transformations are combinations of rotation, scaling, and translation applied to coordinate axes in n-dimensional spaces. A transformation is denoted by q, with $q(S)$ representing the transformed set of points S. The general form of an affine transformation can be expressed as

$$q(p_x, p_y) = \begin{bmatrix} a & b \\ c & d \end{bmatrix} \begin{bmatrix} p_x \\ p_y \end{bmatrix} + \begin{bmatrix} e \\ f \end{bmatrix} = \begin{bmatrix} a \cdot p_x + b \cdot p_y + e \\ c \cdot p_x + d \cdot p_y + f \end{bmatrix}. \quad (3)$$

In this transformation, the coefficients a, b, c, d, e, and f are real numbers that define the parameters. If the translation, scaling, and rotation associated with the mapping q are predetermined, the values of these coefficients are given as

$$\begin{aligned} a = u\cos\theta,\, b = -v\sin\varphi, \\ c = u\sin\theta\,,\ d = v\cos\varphi, \end{aligned} \quad (4)$$

In this context, u represents the scaling factor along the x-axis, v is the scaling factor along the y-axis, θ is the rotation angle about the x-axis, φ is the rotation angle about the y-axis, e and f represent the translations along the x- and y-axis, respectively.

To define an IFS, the concept of contractivity is introduced as following:

Definition 1 (Contractivity) [9] Let S be a metric space with metric f_q . A mapping $q: S \to S$ is said to be Lipschitz with a Lipschitz factor s if there exists a positive real value s such that

$$f_q\big(q(\mathbf{p}_1), q(\mathbf{p}_2)\big) \leq s \cdot f_q(\mathbf{p}_1, \mathbf{p}_2) \quad (5)$$

for all $\mathbf{p}_1, \mathbf{p}_2 \in S$. If the Lipschitz factor satisfies $s < 1$, then q is considered contractive with contractivity s.

An IFS consists of a finite collection of contractive affine transformations. This collection of transformations W defines a mapping from the original image S to the transformed image $Q(S)$, which can be expressed as

$$Q(S) = \cup_{i=1}^{n} q_i(S_i). \quad (6)$$

It is important to note that the contractive affine transformation q_i operates on a subset of the original image S, referred to as block S_i. Consequently, $Q(S)$ is formed as a union of these individual contractive transformations. Each transformation q_i is associated with a predetermined property that determines the significance relative to the other transformations.

To establish a systematic method for identifying the affine transformation that generates the IFS encoding of a desired image, the following two theorems are introduced: the collage theorem and contractive-mapping fixed-point theorem.

Theorem 1 (Collage Theorem) [15] Let S be a complete metric space and $q: S \to S$ be a contractive mapping with a contractivity factor s for any pixel $\mathbf{p} \in S$. Then, the following inequality holds:

$$f_q\big(\mathbf{p}, q^n(\mathbf{p})\big) \leq \frac{1}{1-s} f_q\big(\mathbf{p}, q(\mathbf{p})\big), \quad (7)$$

where $q^n(\cdot)$ represents the n^{th} iteration of the affine transformation.

Theorem 2 (Contractive-Mapping Fixed-Point Theorem) [15] Under the assumption of the collage theorem, there exists a unique point $\mathbf{p}_f \in S$ such that for any point $\mathbf{p} \in S$,

$$\mathbf{p}_f = q(\mathbf{p}_f) = \lim_{n\to\infty} q^n(\mathbf{p}). \quad (8)$$

This point $\mathbf{p}_f$ is referred to as the fixed point or the attractor of the mapping q.

For a contractive affine mapping, the distance $f_q(\mathbf{p}, q^n(\mathbf{p}))$ between the original points and their mapped counterparts decreases with each iteration. Similarly, for an input image S, it can be demonstrated that the error between the original point and the mapped point remains below a certain bound after n iterations. This is established through repeated application of the triangle inequality and the contractivity of q [9]. If the mapped image $q(S)$ exhibits lower complexity than the original image, then q can be viewed as a lossy encoding of S. We refer to such a transformation w within S that satisfies (5) and (6) as a fractal code for the original image S, indicating that S is self-transformable under q. The process exemplifies a common method for constructing fractal objects.

3.3.2 Partitioned Iterated Function System

In the fractal processing approach used in this study, a key requirement is that the width and length of the target area must be equal, with the side length of the scanned image being a power of 2. Once these conditions are met, the partitioned iteration function system (PIFS) can be applied, which generalizes the standard IFS method. In a PIFS, the original image is divided into numerous non-overlapping square blocks of two different sizes, creating a two-level square partition, commonly referred to as quadtrees. The large blocks of the original image, measuring $L_p \times L_p$, are designated as parent blocks, while the smaller ones, measuring $L_p/2 \times L_p/2$, are termed child blocks. Each parent block can be partitioned into four non-overlapping child blocks that correspond to its four quadrants.

During the transformation process, a segment of the original image S, denoted as S_i^q, is transformed into a corresponding section of the reproduced image, represented as R_i, through the mapping q_i. Here, S_i^q is referred to as a domain block and R_i is called a range block. The collection of domain blocks $\{S_i^q\}_{0 \leq i < n}$ is termed the domain pool. The decisions to split a parent block occurs during the encoding of individual image blocks. A metric that measures the difference between the original block and the transformed block is essential for determining whether a split is necessary. This process is repeated until the difference between the original and the approximated image is below a predefined threshold.

Based on this recursive approach, given an image S of the construction site and a collection of n contractive mappings q_1, q_2, …, q_n, the representation of the transformed image of the site can be written as

$$Q(S) = q_1(S) \cup q_2(S) \cup \cdots \cup q_n(S) = \cup_{i=1}^{n} Q_i(S). \quad (9)$$

The partition created in this manner is dependent on the specific image taken from the construction site being processed. This technique enables the encoder to utilize larger blocks in less complex regions of the image while employing smaller blocks to capture finer details in more complex areas.

3.3.3 Fractal Encoding Procedure of FQA

The proposed FQA partitioning algorithm assumes that the images captured from construction sites exhibit fractal characteristics. A key aspect of fractal image processing is minimizing the difference between the original image and its processed result. The goal PIFS encoding process is to identify a set of mappings that reduces this difference between partitioned results and original site conditions with a predefined threshold. The encoding procedure is governed by two main parameters: the tolerable deviation e_t between the original image and the approximated result and the depth (or the finest resolution) r_{min} of the quadtree. The tolerable deviation e_t defines the acceptable deviation between the encoded partitions and the actual image captured at the construction site. The depth of the quadtree determines how much detail is preserved in the transformed partitions, allowing for adaptive grid size based on the visual complexity of different areas.

The coarse image, captured from the construction site, is initially divided into several sections based on a predefined minimum number of grid cells. This quadtree partitioning method represents the image as a hierarchical structure, where each node corresponds to a square section (parent block) of the image, which can be further subdivided into four sub-sections (child blocks). The encoding process begins at the root node, which represents the entire initial image. The relationships among these nodes are structured in a tree-like format, where each node in the branches corresponds to a part of the processed image, or a range block.

After partitioning the image, the range blocks (nodes) are compared with domain blocks from a predefined domain pool $\{S_i^q\}_{0 \le i < n}$. An affine transformation is applied to find the best match that minimizes the difference between the range block and its corresponding domain block. Each domain block, consisting of four non-overlapping square blocks, is four times the size of the range block. To compare them, the pixels in the domain block are averaged in groups of four, reducing the domain block to match the size of the range block.

If the difference between the range block and the domain block exceeds the preset error threshold e_t and the distance between adjacent pixels is larger than the defined minimum resolution r_{min}, the range block is further subdivided into four child blocks, and the process repeats. If the difference is within the acceptable threshold, the affine transformation q_i is stored for that domain block. This collection of all such transformations $Q = \cup q_i$ forms the encoding process of the targeted area, allowing for adaptive grid resolution across different sections of the site based on visual complexity.

Once the area is partitioned into blocks, drones can be deployed accordingly: larger grid blocks correspond to higher flight GSDs, while smaller grids represent lower flight altitudes. Drones are assigned to these grids based on altitude requirements. The blocks, varying in size, are sorted by their proximity to optimize the drones' flight paths. As a result, the flight trajectories at different altitudes can be determined. Taking this into account, the number of drones N_D can be determined and allocated to the appropriate altitudes. Figure 4 illustrates the deployment of drones at different altitudes, tailored to the resolution needed for the partitioned blocks. This approach significantly reduces the number of high-resolution images required, thereby speeding up the overall scanning process for the targeted construction site.

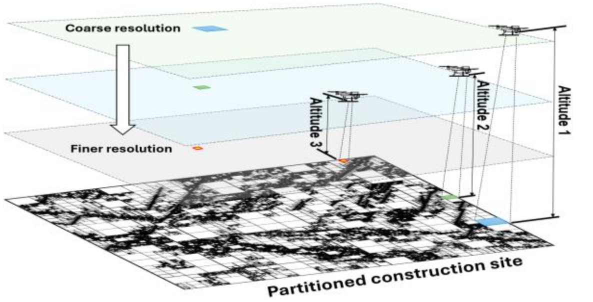

Figure 4. Partitioned construction site and its corresponding drone flight altitudes.

4 Simulation of Different Approaches

To evaluate the performance of the three approaches, a real construction site image covering an area of 64 m × 64 m, as shown in Figure 5, was used to develop a simulated test case. The target resolution was set to a 2 m visible range, based on the downward-facing camera equipped on the drone. This resolution allowed the construction site to be divided into a grid of 32 × 32 cells for both the random walk and zigzag methods.

4.1 Random Walk Approach

In the random walk approach, the number of steps required to fully scan the entire targeted area can vary significantly due to the drone's unpredictable movements. To assess the variability, simulations were conducted using both one drone and two drones. Each scenario was simulated over 200 trials to ensure that the results exhibited Gaussian distribution. The simulated outcomes are presented in Table 2. The random walk method proved to be highly inefficient. A single drone required over 26,000 steps to cover all 1,024 cells of the 32 × 32 grid at least once. Even with two drones working in tandem, the required steps remained high, exceeding 13,000 to ensure full coverage of the grid. These results demonstrate that, while multiple drones can reduce the total steps, the random walk approach is still suboptimal and time-consuming for large-scale site inspections.

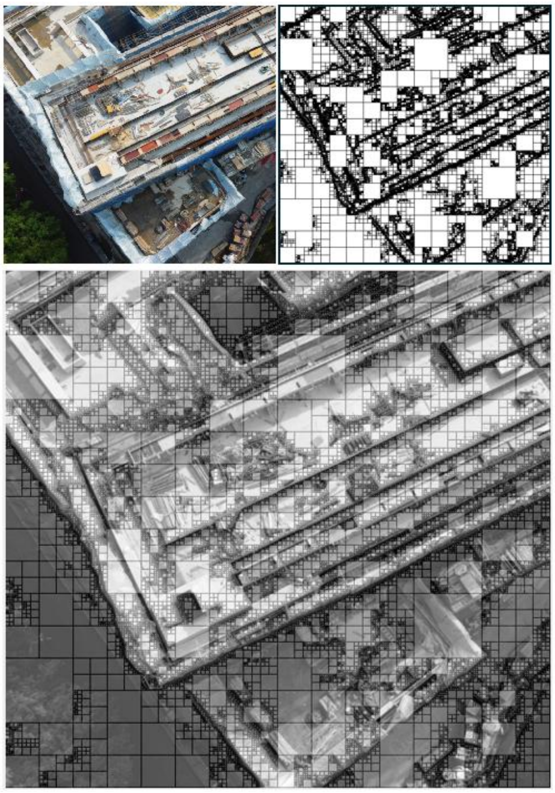

Figure 5. The acquired image of the construction site and the partitioned result (e_t = 10% of the maximum and minimum grayscale values).

4.2 Zigzag Flight Path Planning

Of the simulated approaches, the zigzag approach was the most efficient method for completing a full scan with a fixed resolution. A single drone covered the entire 32 × 32 grid in 1,024 steps, much fewer in comparison to the random walk method. When two drones were deployed, the required steps were halved to 512 for full coverage (with the drones positioned at specific initial locations within the partitioned blocks). This positioning ensures that the zigzag trajectories in each block can be completed systematically and without overlap. Table 3 presents the required steps for areas partitioned into varying grid sizes, highlighting the efficiency and predictability of the zigzag approach compared to the random walk method. This structured deployment helps to ensure optimal utilization of drone resources while maintaining comprehensive coverage.

Table 2 Required steps for a complete scan on the targeted area using random walk method (32× 32 cells).

	Number of drones			
	1		2	
Completed area	Average steps	Standard deviation	Average steps	Standard deviation
50%	2479.6	716.8	1110.1	412.9
70%	4371.8	1066.1	1987.7	678.0
95%	10612	2493	5594.8	1596.7
100%	26502	8901	13585	4479

Table 3 Required steps for a complete scan on the targeted area using zigzag method.

	Number of drones		
	1	2	4
Gridded cells	Required steps	Required steps	Required steps
32 × 32	1024	512	256
64 × 64	4096	2048	1024

4.3 Quadtree Approach

In FQA simulated approach, the number of cells that required drones to visit and acquire images varied, depending on the complexity on the site surface.

4.3.1 Parameters of Fractal Quadtree Approach

To evaluate the performance of the proposed fractal-based path planning approach, images of the College of Liberal Arts Building construction at the National Taiwan University were again used. The area, measuring approximately 64 m × 64 m, was captured, as shown in Figure 5. Before deploying the drones to scan the site and assigning specific flight paths, a preliminary image of the construction site was taken to determine how the area should be partitioned. Once the image was obtained, it was first converted from color to grayscale, a necessary step for FQA. For this test, the construction site was initially divided into 64 blocks, each measuring 8 m × 8 m, to ensure that no portions of the site were scanned without adequate pixel-per-meter resolution. The tolerable deviation e_t was set at 10% of the maximum and minimum grayscale values in the image. Using this threshold, the fractal quadtree approach was applied to generate the partitioned grids for flight scanning, ensuring an optimized balance between resolution and scan efficiency.

4.3.2 Partitioned Blocks Using FQA

The results showed that a simulated construction site could be efficiently partitioned into grids to plan drone flight paths, as demonstrated in Figure 5 and Figure 6.

Initially, the site was divided into very fine grids with a 0.25 m visible range. The original image of the construction site had a resolution of 8 pixels per meter. When partitioned into 8 m × 8 m blocks, the resolution increased to 64 pixels per meter. Doubling the resolution to 128 pixels per meter requires the blocks to be 4 m × 4 m. For this study, the blocks were divided into 2 m × 2 m to achieve the desired resolution of 256 pixels per meter. After merging, the final partitioning resulted in six 8 m × 8 m blocks, 44 blocks sized 4 m × 4 m, and 784 blocks of 2 m × 2 m. This totaled 834 blocks that needed to be scanned and imaged by the drones. In comparison, a traditional zigzag approach for the same area would require scanning 1,024 locations with a single drone, meaning the FQA reduced the total imaging time (no flight time) by approximately 18.75%, requiring only 81.25% of the zigzag approach's locations to be visited.

If the visible range is further refined to 1 m × 1 m blocks, the zigzag approach would require scanning 4,096 locations, while FQA reduces this number to 2,647, or 64.6% of the total grids. At even higher resolutions, 0.5 m × 0.5 m blocks, the FQA covers only 47.91% of the total grids, significantly reducing the imaging effort compared to the zigzag flight path planning method.

Table 4 provides a comparison of the required number of blocks for different visible ranges. Results show that as the resolution becomes finer, FQA substantially reduces the number of locations that need to be scanned, showcasing its efficiency over the zigzag approach. This reduction in the number of required blocks is the key advantage of the FQA, particularly when fine visible range is essential.

Table 4 Comparison of visited blocks and ratios across different tolerable deviations and visible ranges.

e_t	10%			15%		
Visible range	# of blocks	Ratio (%)	PSNR	# of blocks	Ratio (%)	PSNR
2 m × 2 m	832	81.3	24.08	778	76.0	22.84
1 m × 1 m	2647	64.6	25.59	2305	56.3	25.85
0.5 m × 0.5 m	7849	47.9	28.44	6283	38.4	26.04

The quality of the acquired images at different GSDs can be assessed using peak signal-to-noise ratio (PSNR) during the reconstruction of the site image by stitching all partitioned images. To ensure acceptable image fidelity, the PSNR value should typically remain above 25 dB [10]. In this study, the PSNR exceeds 25.59 dB when the compression ratio is kept below 65%, indicating minimal loss of critical visual details.

4.3.3 Synthesis of Flight Paths Using FQA

In FQA, the construction site was partitioned into grids of varying sizes based on the complexity of the acquired images, with smaller grids indicating more detailed areas and larger grids representing fewer complex regions. Once the partitioning was completed, the flight paths for the drones were generated by assigning drones to fly at corresponding altitudes, where the altitude was correlated with the size of the grids. These results indicate that drones flying at higher altitudes can cover larger, less complex areas represented by the bigger grids, while drones flying at lower altitudes can be tasked with scanning smaller, more detailed areas. This adaptive use of altitude ensures that drones are optimally deployed according to the resolution requirements of each specific region within the site.

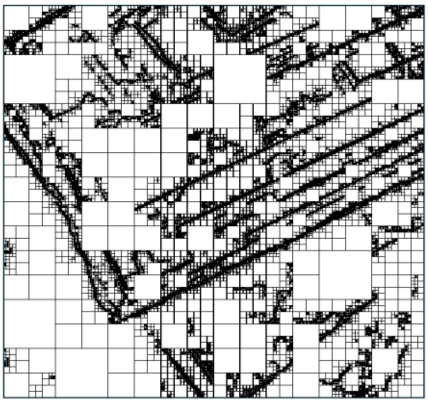

Figure 6. The partitioned result of the construction site ($e_t = 15\%$ of the maximum and minimum grayscale values).

The key advantage of the FQA approach is its efficiency. Drones at higher altitudes can scan large sections of the site in less time, as the lower level of visual detail in these areas requires fewer images. By covering more ground per flight, these drones reduce the total number of paths needed to fully scan the site. Meanwhile, drones operating at lower altitudes can focus on areas that require a higher resolution due to their complexity, ensuring that detailed information is captured where necessary. This distribution of tasks allows for a balanced and scalable operation, where drones can be deployed in the most efficient manner possible based on visual complexity of different zones.

By leveraging the flexibility of flying at different altitudes, FQA may reduce the overall time needed for site scans compared to the two traditional methods. Drones do not need to uniformly fly at low altitudes across the entire site, which can be time-consuming and inefficient. Instead, they can be selectively allocated to specific altitudes, aligning their flight paths with the partitioned grid sizes. This not only reduces the total number of flight paths but also minimizes redundant scanning, allowing for faster coverage of the site without compromising the quality of the images in critical areas. As a result, the overall scan time for the construction site can potentially be reduced, maximizing both the efficiency and precision of the hazard inspection process.

5 Conclusion

The proposed FQA approach offers an efficient and scalable solution for drone-based construction site inspections. By dynamically adjusting grid sizes based on the complexity of acquired images, the FQA approach allows for optimized flight path planning and reduces the time required to scan large areas without sacrificing image quality in critical regions. The adaptive nature of the fractal quadtree technique also enables drones to be deployed at varying GSDs, further enhancing the efficiency of the scanning process by aligning drone altitude with the complexity of the targeted area. This approach not only outperforms traditional approaches such as zigzag and random walk flight patterns but also provides greater flexibility in handling diverse site conditions. Ultimately, the fractal-based grid partitioning method presents a robust and practical solution for improving hazard identification and monitoring on construction sites, facilitating efficient inspections.

6 Acknowledgement and Disclaimer

The authors would like to extend their gratitude to Dr. Jacob J. Lin and Ms. Phuong Linh Le in the National Taiwan University for their valuable support in providing the drone and UAV photographs of the construction sites. The findings and conclusions in this manuscript are those of the authors and do not necessarily represent the official position of NIOSH, CDC. Mention of any company or product does not constitute endorsement by NIOSH, CDC. This activity was reviewed by the CDC, deemed research not involving human subjects, and was conducted consistent with applicable federal law and CDC policy (§See, e.g., 45 C.F.R. part 46; 21 C.F.R. part 56; 42 U.S.C. §241(d), 5 U.S.C. §552a, 44 U.S.C. §3501 et seq).

References

[1] Elghaish F., Matarneh S., Talebi S., Kagioglou M., Hosseini M. R., and Abrishami S. Toward digitalization in the construction industry with immersive and drones technologies: a critical literature review. *Smart and Sustainable Built Environment*, 10(3): 345-363, 2021.

[2] Liang C. J., Le T. H., Ham Y., Mantha B. R., Cheng M. H., and Lin J. J. Ethics of artificial intelligence and robotics in the architecture, engineering, and construction industry. *Automation in Construction*, 162: 105369, 2024.

[3] Lin J. J., Han K. K., and Golparvar-Fard M. A framework for model-driven acquisition and analytics of visual data using UAVs for automated construction progress monitoring. In *Computing in civil engineering 2015*. 156-164, Austin, TX, 2015.

[4] Lin J. J., Ibrahim A., Sarwade S., and Golparvar-Fard M. Bridge inspection with aerial robots: Automating the entire pipeline of visual data capture, 3D mapping, defect detection, analysis, and reporting. *Journal of Computing in Civil Engineering*, 35(2): 04020064, 2021.

[5] Shanti M. Z., Cho C. S., de Soto B. G., Byon Y. J., Yeun C. Y., and Kim T. Y. Real-time monitoring of work-at-height safety hazards in construction sites using drones and deep learning. *Journal of safety research*, 83: 364-370, 2022.

[6] Irizarry J., Gheisari M., and Walker B. N. Usability assessment of drone technology as safety inspection tools. *Journal of Information Technology in Construction*, 17(12): 194-212, 2012.

[7] Yang C. H., Tsai M. H., Kang S. C., and Hung C. Y. UAV path planning method for digital terrain model reconstruction–A debris fan example. *Automation in Construction*, 93:214-230, 2018.

[8] Saeed R. A., Omri M., Abdel-Khalek S., Al E. S., and Alotaibi M. F. Optimal path planning for drones based on swarm intelligence algorithm. *Neural Compu. and Appl.*, 34(12): 10133-10155, 2022.

[9] Fisher Y. *Fractal Image Compression: Theory and Application*. Springer-Verlag, New York, 1995.

[10] Cheng M. H. M., Chiu G. T. C., and Reifenberger R. Fractal compression and adaptive sampling: reducing the image acquisition time in scanning probe microscopy. *Scanning: The Journal of Scanning Microscopies*, 30(6): 463-473, 2008.

[11] Cheng M. H. M. and Bakhoum E. G. Fractal compression and adaptive sampling with HV partitioning: accelerating the scanning process in scanning probe microscopy. In *ASME International Mechanical Engineering Congress and Exposition*, pages 195–201, St. Louis, MO, 2009.

[12] Pinzi M., Galvan S., and Rodriguez y Baena F. The Adaptive Hermite Fractal Tree (AHFT): a novel surgical 3D path planning approach with curvature and heading constraints. *Int. J. of Computer Assisted Radiology and Surgery*, 14: 659-670, 2019.

[13] Sadat S. A., Wawerla J., and Vaughan R. Fractal trajectories for online non-uniform aerial coverage. In *2015 IEEE international conference on robotics and automation (ICRA)*. 2971-2976, Seatle, WA, 2015.

[14] Tai D. and Altschuld J. *Drone Technology in Architecture, Engineering and Construction: A strategic Guide to Unmanned Aerial Vehicle Operation and Implementation*. John Wiley & Sons, New Jersy, 2021.

[15] Jacquin A. E. A novel fractal block-coding technique for digital images. In *IEEE ICASSP Proceeding*, 2225–2228, Albuquerque, NM, 1990.